

# The Effect of the Fast-Flavor Instability on Core-Collapse Supernova Models

TIANSHU WANG <sup>1</sup> AND ADAM BURROWS <sup>2</sup>

<sup>1</sup>*Department of Physics, University of California, Berkeley, CA, 94720-7300 USA*

<sup>2</sup>*Department of Astrophysical Sciences, Princeton University, NJ 08544, USA; School of Natural Sciences, Institute for Advanced Study, Princeton, NJ 08540*

(Dated: Received February 28, 2025)

## ABSTRACT

Merging our supernova code FORNAX with the Box3D fast-flavor neutrino oscillation formalism, we explore the effects of fast-flavor conversion (FFC) in state-of-the-art 1D and 2D core-collapse supernova simulations. We find that after a few tens of milliseconds after bounce the FFC emerges just interior to and exterior to the stalled shock wave. It does not obtain in the PNS core nor near the average neutrinosphere radii. Interior to the shock, this results in a temporary change in the net neutrino heating rate of  $\sim 10\%$ , due mostly to a hardening of the  $\nu_e$  and  $\bar{\nu}_e$  neutrino spectra, despite the decrease in their corresponding neutrino number fluxes. In 1D, the hydrodynamic effects are not large, with increases in the stalled shock radius by of order ten to twenty kilometers that abate within a few hundred milliseconds. In 2D, the hydrodynamic effect of the FFC is a bit more noticeable, resulting in slightly earlier explosions for models for lower-mass progenitors, but also potentially inhibiting explosions for some higher-mass progenitors. Fast-flavor conversion continues to operate at larger radii at later times. The net result is a shift upward in the  $\nu_\mu$  energy and number luminosities and a shift downward in the same quantities for both the  $\nu_e$  and  $\bar{\nu}_e$  neutrinos. There seems to be a trend at very large radii and later times towards partial species and spectral equipartition. If this is true, it could be an interesting feature of supernova neutrino detection at later times in underground and under-ice facilities.

*Keywords:* stars - supernovae - general

## 1. INTRODUCTION

Neutrinos have been considered the central driving agents of the mechanism of the supernova explosions of massive stars since the pioneering work in of Colgate & White (1966) and Arnett (1967) in the 1960's. The concept of the delay in the “ignition” of the explosion after the bounce at nuclear densities of the Chandrasekhar core birthed in a massive star at its terminal phase was advanced by Wilson (1985) and Bethe & Wilson (1985). Though the posited necessary boost in the driving neutrino luminosity due to doubly-diffusive “neutron fingers” was shown not to occur (Bruenn & Dineva 1996), it was later demonstrated that neutrino-driven convection could facilitate explosion (Herant et al. 1994; Burrows et al. 1995a; Janka & Mueller 1996), in particular aided by the turbulent stress of neutrino-driven convection (Burrows et al. 1995a). Since this foundation was laid, there has been an avalanche of investigations over the ensuing decades on all aspects of core collapse and explosion, with the result that the field has matured into a vigorous, if complicated, branch of astrophysics. Recent detailed three-dimensional radiation/hydrodynamic simulations (Lentz et al. 2015; Burrows et al. 2019; Vartanyan et al. 2019a; Müller et al. 2019; Stockinger et al. 2020; Burrows et al. 2020; Bollig et al. 2021; Sandoval et al. 2021; Nakamura et al. 2022; Vartanyan et al. 2023; Burrows et al. 2024a) have demonstrated the viability of the neutrino mechanism and the complexity of the phenomenon (Janka 2012; Burrows 2013; Burrows & Vartanyan 2021; Janka 2025).

However, in order to make progress, this very complexity has necessitated approximations, however modest, to the physical inputs and numerical algorithms. One aspect of neutrino physics whose consequences for supernova explosions and their products has been hovering unresolved is neutrino flavor oscillation, the possibility that neutrinos of different flavors could mix or swap. Since neutrino-matter interactions and production are flavor- and energy-dependent, flavor mixing could change explosion hydrodynamics. Given that in every decade our understanding of supernova physics has co-evolved with our understanding of neutrino physics (Burrows 2018), it is natural that the potential effects of neutrino oscillations need to be understood.

One modality of neutrino oscillation that has recently come into sharp focus is “fast-flavor instability/fast-flavor conversion” (FFI/FFC) and angular crossing, whereby fast neutrino flavor transformations occur where the angular distributions of  $\nu_e$  and  $\bar{\nu}_e$  cross. Such electron-lepton number (ELN) crossing was suggested in the seminal works of Samuel (1993) and Sawyer (2005, 2016), but it took several years for the community to realize its potential importance. Now, there is a rich literature on its physics (Chakraborty et al. 2016; Johns et al. 2020; Padilla-Gay et al. 2022; Richers & Sen 2022; Morinaga 2022) and quantum kinetics (QKE) (Volpe 2015; Richers et al. 2019; Volpe 2024), as well as on an interesting collisional instability (Johns 2023a).

However, to date there has been no calculation embedding the ELN (or “X”LN) into a sophisticated supernova code. The major reason is that multi-group, multi-species and *multi-angle* radiation/hydrodynamic simulations in three spatial dimensions and for all the density matrix elements, including the off-diagonal terms that capture the quantum coherence and mixing (Strack & Burrows 2005; Volpe 2015; Richers et al. 2019; Volpe 2024), have not been possible. Angular-moment methods that require higher-order closures have been developed (Zhang & Burrows 2013; Johns et al. 2020; Nagakura et al. 2021a; Myers et al. 2022; Froustey et al. 2024b; Kneller et al. 2024), but even they have proven too resource-intensive to employ. Importantly, the inverse timescale for FFI is  $\sim\sqrt{2}G_F n_L$ , where  $n_L$  is the background lepton density and  $G_F$  is the Fermi coupling constant, and this in the supernova core can be nanoseconds. Such a timescale is much smaller than the computational timesteps of modern supernova codes (typically microseconds), making the inclusion of FFC and its effects quite difficult. There have been attempts to identify where in the supernova core angular crossings could occur (Abbar et al. 2019; Glas et al. 2020; Morinaga et al. 2020; Abbar et al. 2021; Johns & Nagakura 2021; Nagakura et al. 2021a), some quite sophisticated (Richers et al. 2021a,b), but these have not proven definitive. There have also been attempts to perform simple supernova simulations with approximate models of the effects of FFC (Stapleford et al. 2020; Xiong et al. 2023; Ehring et al. 2023a,b; Zaizen et al. 2024; Mori et al. 2025). These generally make unsubstantiated assumptions about flavor mixing and where it occurs and too have fallen short.

Where there has been progress is in developing approximate schemes that capture the basic physics of angular crossing and FFC, while preserving the basic symmetries. These methods (Xiong et al. 2023; George et al. 2024; Richers et al. 2024, 2022) predict the asymptotic states of fast neutrino-flavor conversion and provide survival probabilities that can be incorporated into modern supernova codes. Also developed are potentially related methods that take a “thermodynamic” or a “maximum entropy” approach (Johns 2023b; Froustey et al. 2024a). Nevertheless, none of these prescriptions has yet been incorporated into a sophisticated supernova code. With this paper, we make the first attempt to do so and to derive the potential consequences of the FFI in supernova hydrodynamics and supernova theory. We employ the Box3D scheme of Richers et al. (2024) that seems adequately to preserve the symmetries of fast-flavor conversion in the context of QKE and to predict survival probabilities that can rather easily be incorporated into modern supernova simulations.

First, in §2 we discuss our computational approach, and how we have generalized our core-collapse supernova (CCSN) code FORNAX to include the Box3D fast-flavor conversion methodology. Then, in §3 we describe our results and explore the differences in the hydrodynamic and neutrino sectors due to the inclusion of fast-flavor oscillations. Finally, we summarize our findings in §4.

## 2. METHOD

The sophisticated code (FORNAX) we use for this study has been described in detail in Skinner et al. (2019), Burrows et al. (2023), and in the appendix to Vartanyan et al. (2019a). The neutrino-matter microphysics used in its classical physics sector can be found in Burrows et al. (2006) and Wang & Burrows (2020). In the past, FORNAX has been used in a variety of papers on a broad spectrum of topics in core-collapse supernova theory (e.g., Radice et al. 2017; Burrows et al. 2018; Vartanyan et al. 2018, 2019b; Morozova et al. 2018; Burrows et al. 2019; Radice et al. 2019; Nagakura et al. 2019; Vartanyan et al. 2019a; Nagakura et al. 2020; Vartanyan & Burrows 2020; Burrows et al. 2020;

Nagakura et al. 2021b; Burrows & Vartanyan 2021; Vartanyan et al. 2022; Coleman & Burrows 2022; Burrows et al. 2023, 2024a). Here, we employ the SFHo nuclear equation of state (Steiner et al. 2013), 1024 radial zones for the 1D simulations, and for the 2D simulations a grid of  $1024 \times 128$  ( $r \times \theta$ ). We use for both sets of simulations twelve neutrino energy groups from 1 to 300 MeV for each of three species ( $\nu_e$ ,  $\bar{\nu}_e$ , and “ $\nu_\mu$ ” ) [ $\equiv \nu_\mu + \bar{\nu}_\mu + \nu_\tau + \bar{\nu}_\tau$ ]]. The outer boundary is set at 30,000 kilometers (km) and the inner radial zone is 0.5 km wide. The progenitor models are taken from Sukhbold et al. (2016) and Sukhbold et al. (2018).

For this study, and to determine the effects of fast-flavor instability and conversion, we have added to our classical FORNAX code the Box3D oscillation formalism (Richers et al. 2024). The Box3D scheme is an approximate method for predicting asymptotic states of fast neutrino-flavor conversion, generalized to handle non-axisymmetric angular distributions. Note that for most of the inner region the timescale for fast-flavor conversion is much shorter than the  $\sim$ microsecond timescale of the hydrodynamic timestep. With the survival probabilities provided we oscillate one neutrino species into another, while preserving the symmetries of fast-flavor conversions in the context of the quantum kinetic equations (Volpe 2015; Richers et al. 2019; Volpe 2024; Kneller et al. 2024). In this method, heavy-lepton flavor neutrinos are assumed to have equal distributions ( $f_{\nu_\mu} = f_{\nu_\tau} = f_{\nu_x}$ ). The same assumption is been made for heavy-lepton flavor antineutrinos ( $f_{\bar{\nu}_\mu} = f_{\bar{\nu}_\tau} = f_{\bar{\nu}_x}$ ). Given the neutrino distribution  $f_{\nu_\alpha}(E, \hat{n})$  (where  $E$  is the neutrino energy and  $\hat{n}$  is the momentum direction vector), the  $\alpha$ -flavor lepton number angular distribution is (for simplicity we assume here  $c = \hbar = 1$ ):

$$G_\alpha(\hat{n}) = \sqrt{2}G_F \int_0^\infty \frac{dE E^2}{(2\pi)^3} (f_{\nu_\alpha}(E, \hat{n}) - f_{\bar{\nu}_\alpha}(E, \hat{n})), \quad (1)$$

and the ELN-XLN distribution in a given direction is

$$G_{\hat{n}} = G_e(\hat{n}) - G_x(\hat{n}). \quad (2)$$

The sign of  $G$  divides the angular space into two regions:  $\Gamma_+ = \{\hat{n}|G(\hat{n}) > 0\}$  and  $\Gamma_- = \{\hat{n}|G(\hat{n}) < 0\}$ . We define integrals on these two regions:

$$I_+ = \int_{\Gamma_+} d\hat{n} G_{\hat{n}}, \quad I_- = - \int_{\Gamma_-} d\hat{n} G_{\hat{n}}. \quad (3)$$

The survival probability  $P(\hat{n})$  is defined as

$$P(\hat{n}) = \begin{cases} \frac{1}{3} & I_- < I_+, \hat{n} \in \Gamma_-, \\ 1 - \frac{2I_-}{3I_+} & I_- < I_+, \hat{n} \in \Gamma_+, \\ \frac{1}{3} & I_- > I_+, \hat{n} \in \Gamma_+, \\ 1 - \frac{2I_+}{3I_-} & I_- > I_+, \hat{n} \in \Gamma_-, \end{cases} \quad (4)$$

and the asymptotic angular distributions are given by

$$\begin{aligned} f_{\nu_e}^a(E, \hat{n}) &= P(\hat{n})f_{\nu_e}(E, \hat{n}) + [1 - P(\hat{n})]f_{\nu_x}(E, \hat{n}), \\ f_{\bar{\nu}_e}^a(E, \hat{n}) &= P(\hat{n})f_{\bar{\nu}_e}(E, \hat{n}) + [1 - P(\hat{n})]f_{\bar{\nu}_x}(E, \hat{n}), \\ f_{\nu_x}^a(E, \hat{n}) &= \frac{1}{2}[1 - P(\hat{n})]f_{\nu_e}(E, \hat{n}) + \frac{1}{2}[1 + P(\hat{n})]f_{\nu_x}(E, \hat{n}), \\ f_{\bar{\nu}_x}^a(E, \hat{n}) &= \frac{1}{2}[1 - P(\hat{n})]f_{\bar{\nu}_e}(E, \hat{n}) + \frac{1}{2}[1 + P(\hat{n})]f_{\bar{\nu}_x}(E, \hat{n}). \end{aligned} \quad (5)$$

The following formula is used to estimate the local growth rate of fast flavor conversion (Morinaga et al. 2020; Nagakura et al. 2024):

$$\sigma = \sqrt{I_+ I_-}, \quad (6)$$

and the change in the neutrino angular distribution per simulation timestep  $\Delta t$  is;

$$f'_{\nu_\alpha} - f_{\nu_\alpha} = -(1 - e^{-\sigma \Delta t})(f_{\nu_\alpha} - f_{\nu_\alpha}^a). \quad (7)$$

The angular moments used by the M1 transport scheme are calculated from such distributions via numerical integrations in the angular space.

Our implementation of Box3D in FORNAX conserves the sum of the neutrino/(anti-neutrino) lepton numbers to machine accuracy. Since our M1 transport scheme (Skinner et al. 2019) evolves only the zeroth and first moments of neutrino angular distributions, an angle-dependent closure relation is needed to reconstruct the full angular distributions. For this purpose we use the Minerbo maximum entropy closure (Minerbo 1978). This closure assumes that the neutrino angular distribution can be written in a two-parameter functional form  $f(\hat{n}) = \exp(a\hat{n} \cdot \hat{f} - b)$ , where  $a$  and  $b$  are parameters derived from the zeroth and first angular moments calculated in FORNAX and  $\hat{f}$  is the direction of the neutrino flux. We have in the past explored the dependence of core-collapse simulations without oscillation effects on the second- and third-moment closure relations employed in M1 and found very little variation (Wang & Burrows 2023). We use Lebedev quadrature on the sphere with 110 points to perform the necessary angular integrations, which integrates exactly all spherical harmonics up to 17th order. The result of these integrations for every spatial point, neutrino species, energy-group, and timestep is a slowdown of FORNAX by a factor of  $\sim 2.0$ .

Furthermore, we note that we are assuming heavy-lepton flavor neutrinos and anti-neutrinos have equal distributions ( $f_{\nu_x} = f_{\bar{\nu}_x}$ ). This assumption allows one to bundle all heavy-lepton neutrinos and anti-neutrinos together as one type, which significantly speeds up the simulations. We note that this assumption allows the indirect mixing between  $\nu_e$  and  $\bar{\nu}_e$  via  $\nu_e \leftrightarrow \nu_x = \bar{\nu}_x \leftrightarrow \bar{\nu}_e$ , but in our tests we find that the total ELN ( $N_{\nu_e} - N_{\bar{\nu}_e}$ ) is conserved within 10%, which indicates that the  $\nu_e$  and  $\bar{\nu}_e$  conversion is not too significant. Therefore, we suggest this is a good first-order approach.

### 3. RESULTS

#### 3.1. Comparison of One-Dimensional Models: With and Without Fast-Flavor Conversion

We have calculated for this study models in both 1D (spherical) and 2D (axisymmetric), with and without fast-flavor conversion à la our FFC scheme. We highlight a few representative progenitors (z9.6, s9.0, s12.25, s14, s18 and s25) taken from A. Heger (z9.6, private communication) and Sukhbold et al. (2016, 2018, s9.0, s12.25, s14, s18, s25). These are a few of the same models employed in our previous 3D studies (e.g., Burrows et al. 2024a; Wang & Burrows 2024). The goals of this investigation are twofold: First, to determine the alterations in the neutrino fields in time and space due to the FFC. Second, to determine the hydrodynamic consequences of these variations. The latter would ostensibly result from changes in the neutrino heating rates due to changes in energy spectra and species mix and due to changes in the shrinkage rate of the proto-neutron star (PNS) core, with the former effect likely predominant. We note that ours are the first CCSN calculations to incorporate a reasonable algorithm for the FFC naturally into a supernova code that also automatically addresses the hydrodynamic and neutrino transport feedbacks.

Generally, as the left hand side of Figure 1 demonstrates, there is a delay of  $\sim \tau_{\text{FFC}}$  of milliseconds (ms) in the onset of the effect of the FFC on the net neutrino heating rate, which lasts for a finite time (hundreds of milliseconds). During this phase the net heating rate in the gain region can be altered by  $\sim 10\%$ . Low mass models show enhanced heating rates, while massive ones show less enhanced heating rates and even slightly decreased heating rates. After that interval, the heating rate behind the shock settles to that without the FFC for the lowest-mass progenitors, but generally lower for the higher-mass progenitors. In 1D, the shock radius, due mostly to the slightly enhanced heating rate behind it, achieves a slightly larger radius (by a few to ten percent), and then recedes in a manner reminiscent of models without the FFC. The right panel of Figure 1 demonstrates this behavior.

Interestingly, even after the heating enhancement in the interior subsides, in the region exterior to the stalled shock and at larger distances the FFC can still operate, particularly as the radiation field becomes more forward-peaked; the mix of neutrino species is altered from what it would be without the FFC. Figure 2 demonstrates the time evolution in 1D of the energy (left) and number (right) luminosities at 10000 kilometers (km) with (solid) and without (dashed) the FFC. Asymptotically, the “ $\nu_\mu$ ” luminosities (blue) are enhanced by a few to  $\sim 10\%$  for the low-ZAMS-mass 9.0  $M_\odot$  progenitor (tapering off to no effect after  $\sim 500$  ms) and by as much as a factor of two for the 18  $M_\odot$  model (not tapering off during the simulation). The corresponding effects of the FFC on the  $\nu_e$  (red) and  $\bar{\nu}_e$  (green) neutrinos are in the opposite direction and of comparable fractional magnitude. They also persist for the more massive progenitor. The differences between the behavior for the 9 and 18  $M_\odot$  models can be traced to the larger mass accretion rates for the more massive (higher compactness (O’Connor & Ott 2011)) star and its continued accretion in 1D.

In addition, species equipartition is not achieved in the gain region relevant to the explosion. However, and importantly, as the right-hand side of Figure 2 indicates, despite the operation of the FFC, species equipartition is approached, but not completely achieved at 10,000 km and later times. We note that “equipartition” in our three

neutrino species case is different from full equipartition. If we had distinguished  $\nu_x$  and  $\bar{\nu}_x$  neutrinos, flavor equipartition would mean  $\nu_e = \nu_x$  and  $\bar{\nu}_e = \bar{\nu}_x$ . In the three-species case, equipartition means that the two species with lower number densities (in our case  $\bar{\nu}_e$  and  $\nu_x$ ) have the same distribution, while the total ELN  $N_{\nu_e} - N_{\bar{\nu}_e}$  is conserved. This is the “equipartition” described by the phenomenological method in [Ehring et al. \(2023a\)](#), and is very similar to what we see at large radii. In our scheme, the neutrinos are no longer mixing at 10000 km, because of the growth rate control in equation 7. Given this, full equipartition (as defined by  $\nu_e = \nu_x = \bar{\nu}_x = \bar{\nu}_e$ , since we assume  $\nu_x = \bar{\nu}_x$ ) will never be reached<sup>1</sup>.

Figure 3 compares the neutrino spectra with and without the FFC for the same two progenitors. When the FFC operates, the  $\nu_\mu$  neutrino spectra are softer and the  $\nu_e$  and  $\bar{\nu}_e$  neutrino spectra are harder. The hardening of the spectra of the electron types compensates in the heating rate for the diminution in their number and energy fluxes due to the operation of the FFC (see left panel of Figure 1).

Interestingly, Figure 4 shows the FFC conversion rate (eq. 6) versus radius at a given time and manifests the roughly power-law behavior at larger radii expected for this quantity ([Morinaga et al. 2020](#)). This demonstrates in part that our algorithm captures the anticipated behaviors and also shows where the FFC emerges. The major important regions in the context of supernova hydrodynamics where the FFC operates are just behind and just above the shock wave. However, as Figure 4 suggests, even when the neutrinos are not coupled to matter the FFC can still occur at larger radii. The FFC does not occur at the base of the gain region, nor in the PNS core.

Model z9.6 is one of the few progenitor models that explodes in 1D ([Wang & Burrows 2024](#)). The right panel of Figure 1 demonstrates that the FFC gives that model a slight boost, causing it to explode a tad earlier and with slightly higher shock speeds. However, the effect in 1D is not large.

### 3.2. Comparison of Two-Dimensional Models: With and Without Fast-Flavor Conversion

We now turn to simulations in 2D, with and without fast-flavor conversions and for the same progenitor models discussed in §3.1. Without the FFC it has long been known that the neutrino-driven turbulence behind the shock wave that emerges in multi-D is central to the explosion of theoretical core-collapse supernovae ([Burrows et al. 1995b](#); [Janka & Mueller 1996](#); [Janka 2012](#); [Burrows 2013](#); [Burrows & Vartanyan 2021](#)). Under this paradigm, most multi-D models now explode effortlessly ([Burrows et al. 2024a](#)). However, how might the FFC alter this narrative? What are the potential effects of flavor changes and neutrino mixing on supernova observables and on the emitted neutrino luminosities themselves? In the context of the FFC and embedding the approach found in [Richers et al. \(2024\)](#) into our workhorse multi-D supernova code FORNAX ([Skinner et al. 2019](#)), we are now in a position to address these questions, if only preliminarily.

Figure 5 depicts on the left the heating rate in the gain region and on the right the mean shock radius versus time. What we see is that the heating rates can differ appreciably for the higher-mass progenitors, while only modestly for the lower-mass progenitors. At early times for the lower-mass progenitors, the heating rates are marginally higher and the evolution of the shock radius reflects this (see also Figure 1). However, for the higher mass progenitors the heating rates at early times for these 2D models are indeed higher. But, since these models generally explode (if they do) later on, it is the heating rates at later times that are germane and these with the FFC are at times lower, at times higher after  $\sim 300$  ms after bounce. One result is that the  $25-M_\odot$  model that explodes in 2D and 3D in our previous work doesn’t here explode in 2D. Whether this is the case in 3D and at higher resolution ([Nagakura et al. 2019](#)), or whether this is some consequence of chaotic stochasticity when the explodability is close, remains to be determined. Nevertheless, this will be an intriguing topic for future exploration.

Figure 6 is the 2D version of Figure 2 and shows quite similar behavior. At late times, equipartition seems to be approached, but at 10000 km is not reached. Though the  $\bar{\nu}_e$  and  $\nu_\mu$  species are close to equipartition, the  $\nu_e$  neutrinos are separate. Nevertheless, at “infinite” radius and if we had distinguished in this study  $\nu_x$  neutrinos from  $\bar{\nu}_x$  neutrinos, there remains the distinct possibility that at least partial species equipartition ( $\nu_x = \nu_e$  and  $\bar{\nu}_x = \bar{\nu}_e$ ) might indeed have been achieved at later times (see footnote in §3.1). If this were the case, the detection and interpretation of supernova neutrinos would be interestingly altered. A very important aspect of future work on the role of the FFC in supernovae will be the investigation of this stunning possibility.

<sup>1</sup> In a more general scheme which doesn’t assume  $\nu_x = \bar{\nu}_x$ , full equipartition (as defined by  $\nu_e = \nu_x$  and  $\bar{\nu}_x = \bar{\nu}_e$  separately) at infinity at late times is likely to be reached. If so, this would have an interesting effect of the detection of supernova neutrinos in underground facilities on Earth, but this still needs to be explored in future investigations.

Figure 7 portrays the same shifts in 2D seen in Figure 3 for 1D. The FFC hardens the  $\nu_e$  and  $\bar{\nu}_e$  neutrinos, while softening the  $\nu_\mu$  neutrinos. Figure 8 depicts the regions in 2D where the FFC operates. At early times, the FFC is clearly more prominent interior to the shock in the gain region, while at later times it does not disappear, though it is more complexly distributed. It remains to be seen what obtains in 3D and when more precise angular information is available. In the interim, the results we obtain are quite interesting and exciting, however preliminary.

#### 4. CONCLUSIONS

In this paper, we have explored the effects of fast-flavor conversion in state-of-the-art 1D and 2D core-collapse supernova simulations incorporating the Box3D algorithm of [Richers et al. \(2024\)](#) into the FORNAX code. We find that after a few tens of milliseconds after bounce the FFC emerges in strength just interior to and just exterior to the stalled shock wave. It does not obtain in the PNS core nor near the average neutrinosphere radii. Interior to the shock, this results in a temporary increase in the net neutrino heating rate, due mostly to a hardening of the  $\nu_e$  and  $\bar{\nu}_e$  neutrino spectra despite the decrease in their corresponding neutrino number fluxes. In 1D, the hydrodynamic effects of this modest enhancement are not large, with temporary increases in the stalled shock radius by of order ten to twenty kilometers that abate within a few hundred milliseconds. However, for the one model (z9.6) that explodes in 1D without the FFC the corresponding model with FFC explodes slightly earlier and slightly more energetically.

Importantly, though any enhancement in the neutrino heating rate itself is confined to the quoted inner regions and earlier times, the FFC itself continues to operate at larger radii and at later times, though with diminishing effect (see Figure 4). The net result is a shift upward in the asymptotic “ $\nu_\mu$ ” energy and number luminosities and a corresponding shift downward in the same quantities for both the  $\nu_e$  and  $\bar{\nu}_e$  neutrinos. In our simulations, this mixing brings the number luminosities closer to, but not to, equipartition at larger radii and later times. The magnitude of the FFC-caused shift in these quantities at a given radius is smaller for the lower-mass/lower-compactness progenitors and larger for the higher-mass/higher-compactness progenitors. However, we speculate that had we distinguished  $\nu_x$  and  $\bar{\nu}_x$  neutrinos and extended our simulation space to much larger radii at least partial species equipartition ( $\nu_x = \nu_e$  and  $\bar{\nu}_x = \bar{\nu}_e$ ) might have emerged. If this is true, it could interestingly influence the detection of supernova neutrinos in underground and under-ice facilities.

In 2D, the hydrodynamic effect of the FFC is a bit more noticeable. For the lower-mass progenitors, turning on the FFC results in slightly earlier explosions than for models that exploded without the fast-flavor effect. We note that such models as the 12.25- and 14- $M_\odot$ , that did not explode in previous calculations in 2D or 3D ([Burrows et al. 2024b](#)), still don’t explode when the FFC is enabled. Whether the same will be true in 3D remains to be seen. Curiously, for higher-mass progenitors (such as the s25 model) in 2D the FFC seems to inhibit explosion. Whether this remains the case in 3D is not yet clear. It will be important to ascertain the effects of the FFC on the raft of supernova observables, including the final explosion energies and nucleosynthetic yields. The latter depend upon the asymptotic electron fraction ( $Y_e$ ), which is determined by the countervailing effects of  $\nu_e$  and  $\bar{\nu}_e$  absorption altered slightly by the FFC-induced shifts in their respective emission characteristics.

As suggested by [Ehring et al. \(2023b\)](#), the residual neutron star mass of the lowest-mass progenitors may be shaved a bit ( $\sim 0.02 M_\odot$ ) relative to that without the FFC. This might help reconcile the apparent gap between the theoretically predicted lowest mass neutron star ( $\sim 1.2$ - $1.25 M_\odot$ , ([Radice et al. 2017](#))) and the lowest measured mass for a neutron star ( $1.174 M_\odot$ , ([Martinez et al. 2015](#))).

The calculations presented in this paper are the first of their kind that couple a classical radiation/hydrodynamics supernova code with a credible algorithm for incorporating fast-flavor conversion between neutrino species to determine the consequences for both supernova hydrodynamics and the emergent neutrino signal. Our results are quite interesting and provocative, but they are only preliminary. Improvements in the FFC algorithm, as well as a new series of 3D simulations incorporating the FFC for a range of progenitors, will be important next steps. Moreover, collisional flavor transformation ([Johns 2023a](#)) and spectral swaps ([Chakraborty et al. 2016](#)) have yet to be similarly vetted. In any case, however imperfect, the insights we have garnered here should now serve to ignite the next generation of studies on this exciting topic at the intersection of supernova theory and neutrino physics.

#### DATA AVAILABILITY

The data presented in this paper can be made available upon reasonable request to the corresponding author.

## ACKNOWLEDGMENTS

We thank David Vartanyan for our long-term productive collaboration and Lucas Johns and Hiroki Nagakura for their many insights into the fast-flavor conversion phenomenon. TW acknowledges support by the U. S. Department of Energy under grant DE-SC0004658, support by the Gordon and Betty Moore Foundation through Grant GBMF5076 and Simons Foundation grant (622817DK). AB acknowledges former support from the U. S. Department of Energy Office of Science and the Office of Advanced Scientific Computing Research via the Scientific Discovery through Advanced Computing (SciDAC4) program and Grant DE-SC0018297 (subaward 00009650) and former support from the U. S. National Science Foundation (NSF) under Grant AST-1714267. We are happy to acknowledge access to the Frontera cluster (under awards AST20020 and AST21003). This research is part of the Frontera computing project at the Texas Advanced Computing Center ([Stanzione et al. 2020](#)). Frontera is made possible by NSF award OAC-1818253. Additionally, a generous award of computer time was provided by the INCITE program, enabling this research to use resources of the Argonne Leadership Computing Facility, a DOE Office of Science User Facility supported under Contract DE-AC02-06CH11357. Finally, the authors acknowledge computational resources provided by the high-performance computer center at Princeton University, which is jointly supported by the Princeton Institute for Computational Science and Engineering (PICSciE) and the Princeton University Office of Information Technology, and our continuing allocation at the National Energy Research Scientific Computing Center (NERSC), which is supported by the Office of Science of the U. S. Department of Energy under contract DE-AC03-76SF00098.

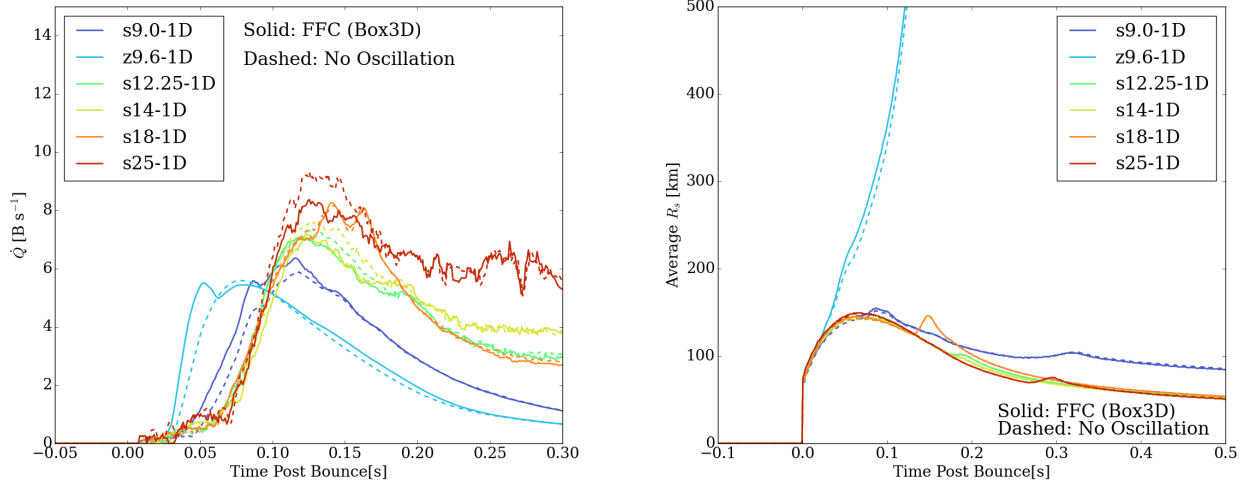


**Figure 1. Left:** The net heating rate (in units of  $10^{51} \text{ erg s}^{-1}$ ) in the gain region behind the shock for 1D simulations using FORNAX of the z9.6, s9.0, s12.25, s14, s18, and s25 progenitor models versus time (in milliseconds) after bounce. The dashed curves are without the Box3D implementation of fast-flavor conversion and the solid curves include it. **Right:** The shock radius versus time after bounce for the models depicted on the left panel of this figure set. In 1D, the inclusion of FFC does not result in a qualitative difference in hydrodynamics, but for the z9.6 model, which does explode in 1D without the FFC, the explosion occurs a bit earlier and a bit more vigorously when FFC effects are included. See text for a discussion of both these panels.



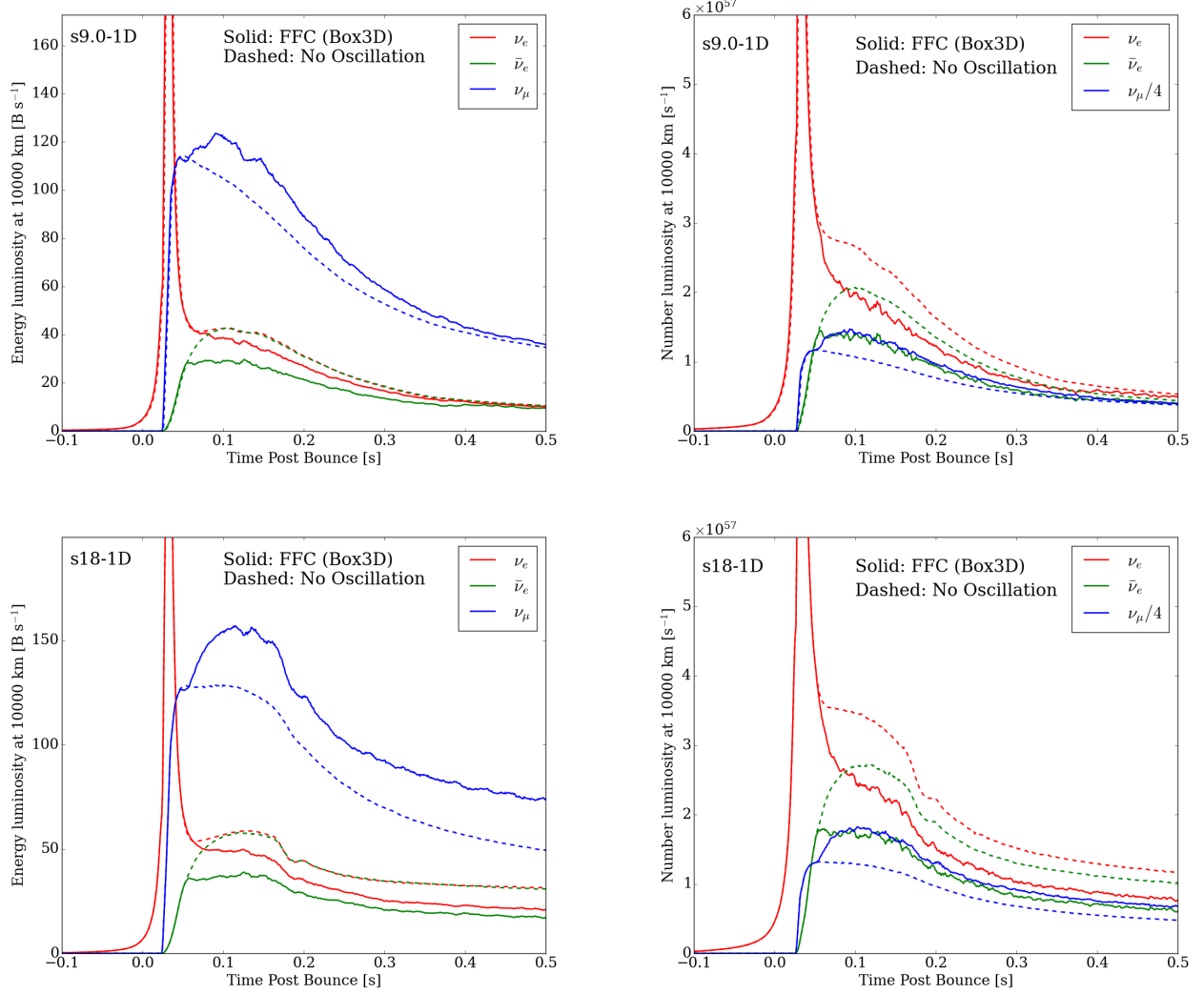


**Figure 2. Left:** The evolution of the neutrino energy luminosities (in units of Bethes ( $10^{51} \text{ erg s}^{-1}$ ) at 10000 km) versus time after bounce (in seconds) for the 9 (top) and 18 (bottom)  $M_\odot$  1D progenitor simulations of Figure 1, with (solid) and without (dashed) the inclusion of the FFC. Note that  $\nu_\mu$  is the combination of  $\nu_\mu, \bar{\nu}_\mu, \nu_\tau,$  and  $\bar{\nu}_\tau$ . After a slight delay, fast-flavor conversion boosts the  $\nu_\mu$  luminosities by as much as 20% for the 9.0  $M_\odot$  (and then tapers off) and by  $\sim 20\%$  for the 18  $M_\odot$  model (maintaining steady during the simulation). Correspondingly, the  $\nu_e$  and  $\bar{\nu}_e$  luminosities are suppressed, conserving total neutrino number. **Right:** The corresponding number luminosities (in units of  $10^{57}$  neutrinos per second) versus time after bounce. For the number luminosity comparison, we show “ $\nu_\mu$ ”/4. While the FFC does redistribute the neutrino species mix, equipartition is not fully achieved in these simulations on our finite grid. See text for a discussion.

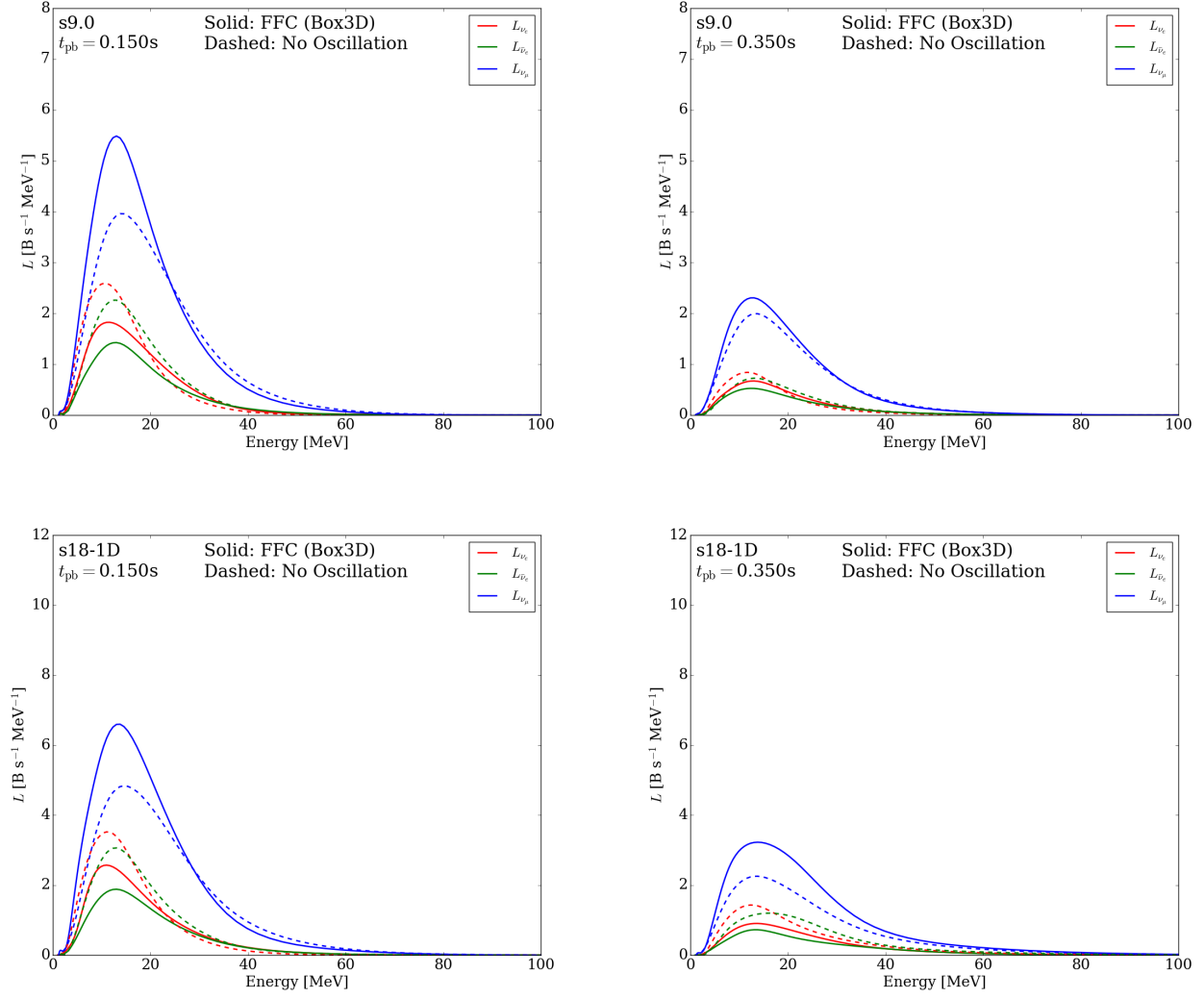


**Figure 3.** The emergent spectra (splined) of the neutrinos, with (solid) and without (dashed) the FFC, for 1D simulations of the progenitors highlighted in Figure 2 and for two times after bounce. Note that  $\nu_\mu$  is the combination of  $\nu_\mu$ ,  $\bar{\nu}_\mu$ ,  $\nu_\tau$ , and  $\bar{\nu}_\tau$ . When the FFC is operative, the  $\nu_\mu$  neutrino spectrum is softened, while both the  $\nu_e$  and  $\bar{\nu}_e$  neutrino spectra harden slightly.

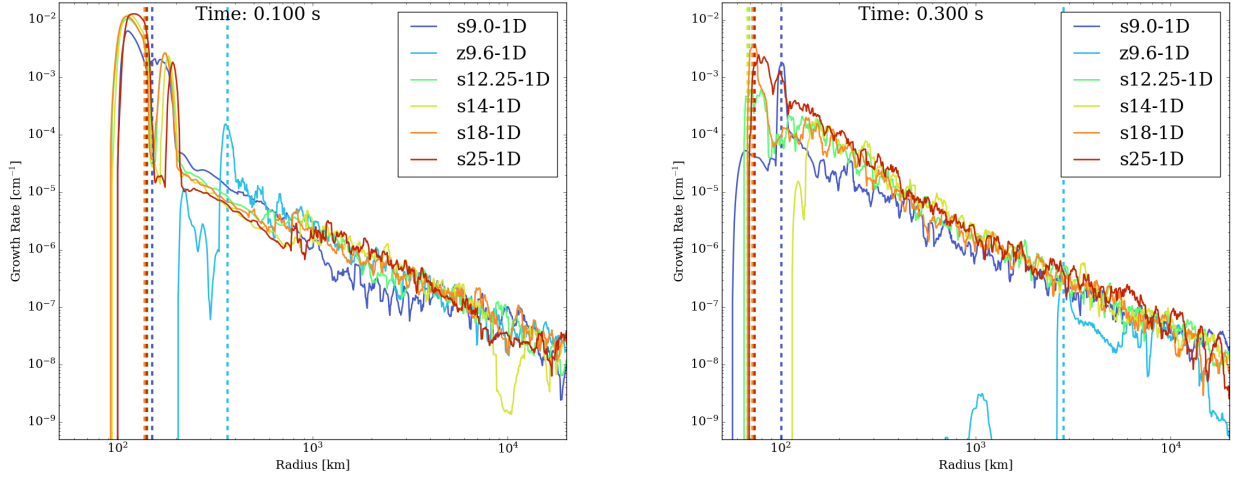


**Figure 4.** The local FFC rate (using eq. 6, in units of  $\text{cm}^{-1}$ ) versus radius for two representative times (100 and 300 milliseconds) after bounce for representative 1D models when the FFC is operating. We have smoothed these curves with boxcar averages in radius (over 10 km) and in time (over 10 ms). The region just interior to and just exterior to the shock wave (vertical dashed line) is where the conversion rate is largest. There is no FFC interior to the outer gain region, either in the proto-neutron star or near the average neutrinospheres. However, at large radii, though there is effectively no neutrino matter heating, the FFC continues, due in no small measure to the progressively more forwardly-peaked angular distribution of the radiation. As this figure demonstrates, the FFC rate at large radii follows a power-law relation. The power-law index is close to  $-(1 + \beta)$  expected in Morinaga et al. (2020), where  $\beta$  is the power index of the density profile exterior to the shock ( $\rho \propto r^{-\beta}$ ).

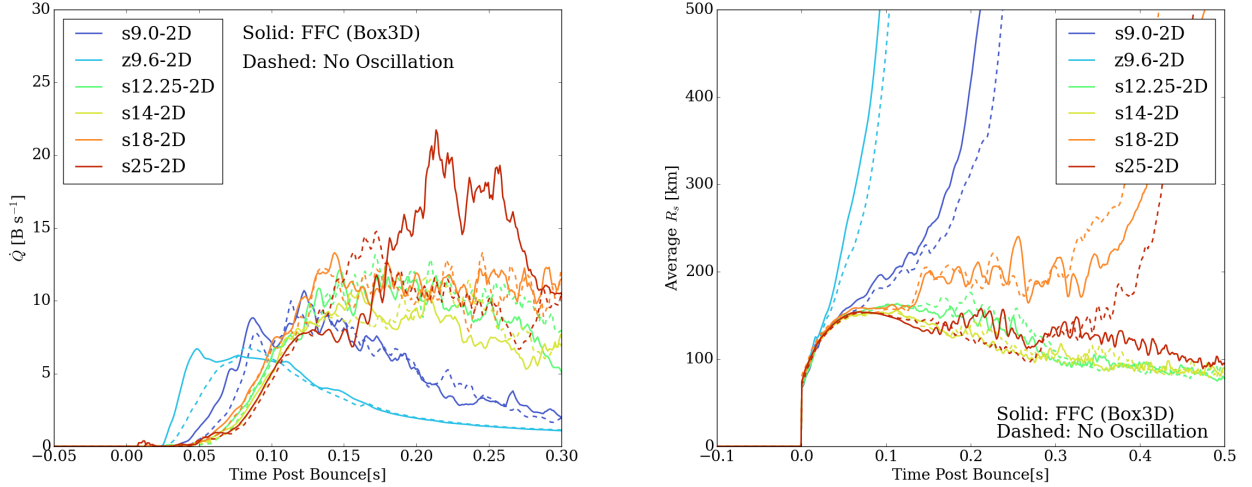


**Figure 5. Left:** The net heating rate (in units of  $10^{51} \text{ erg s}^{-1}$ ) in the gain region behind the shock for 2D simulations of the z9.6, s9.0, s12.25, s14, s18, and s25 progenitor models versus time (in milliseconds) after bounce. The dashed curves are without the Box3D implementation of fast-flavor conversion and the solid curves include it. **Right:** The shock radius versus time after bounce for the models depicted on the left panel of this figure set. The low-mass models explode more promptly with FFC, while the more massive models are less sensitive to it. The s25 model fails to explode if FFC is included. This shows the possibility that FFC may hinder the explosion in more massive models.

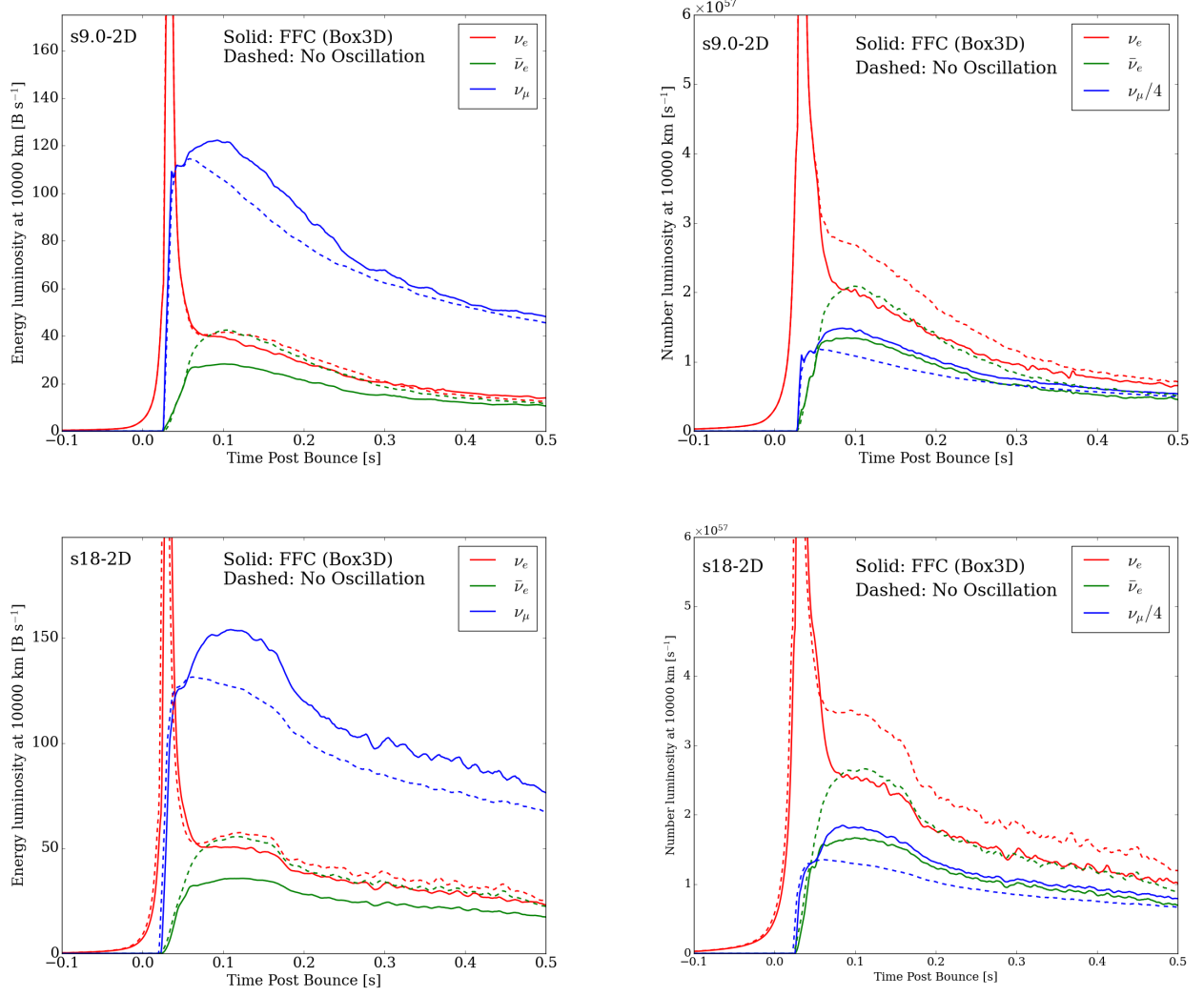


**Figure 6. Left:** The evolution of the neutrino energy luminosities ( $L$ , in units of Bethes ( $10^{51} \text{ erg s}^{-1}$ ) at 10000 km) versus time after bounce (in seconds) for the 9 (top) and 18 (bottom)  $M_\odot$  2D progenitor simulations of Figure 5, with (solid) and without (dashed) the inclusion of the FFC. Note that  $\nu_\mu$  is the combination of  $\nu_\mu$ ,  $\bar{\nu}_\mu$ ,  $\nu_\tau$ , and  $\bar{\nu}_\tau$ . The behaviors are very similar to the corresponding 1D simulations, except that 2D models have higher luminosities at later time than 1D because of proto-neutron star convection (Nagakura et al. 2020). **Right:** The corresponding number luminosities (in units of  $10^{57}$  neutrinos per second at 10000 km) versus time after bounce. For the number luminosity comparison, we show “ $\nu_\mu$ ”/4. While the FFC does redistribute the neutrino species mix, equipartition is not fully achieved in these simulations on our finite grid. See text for a discussion.

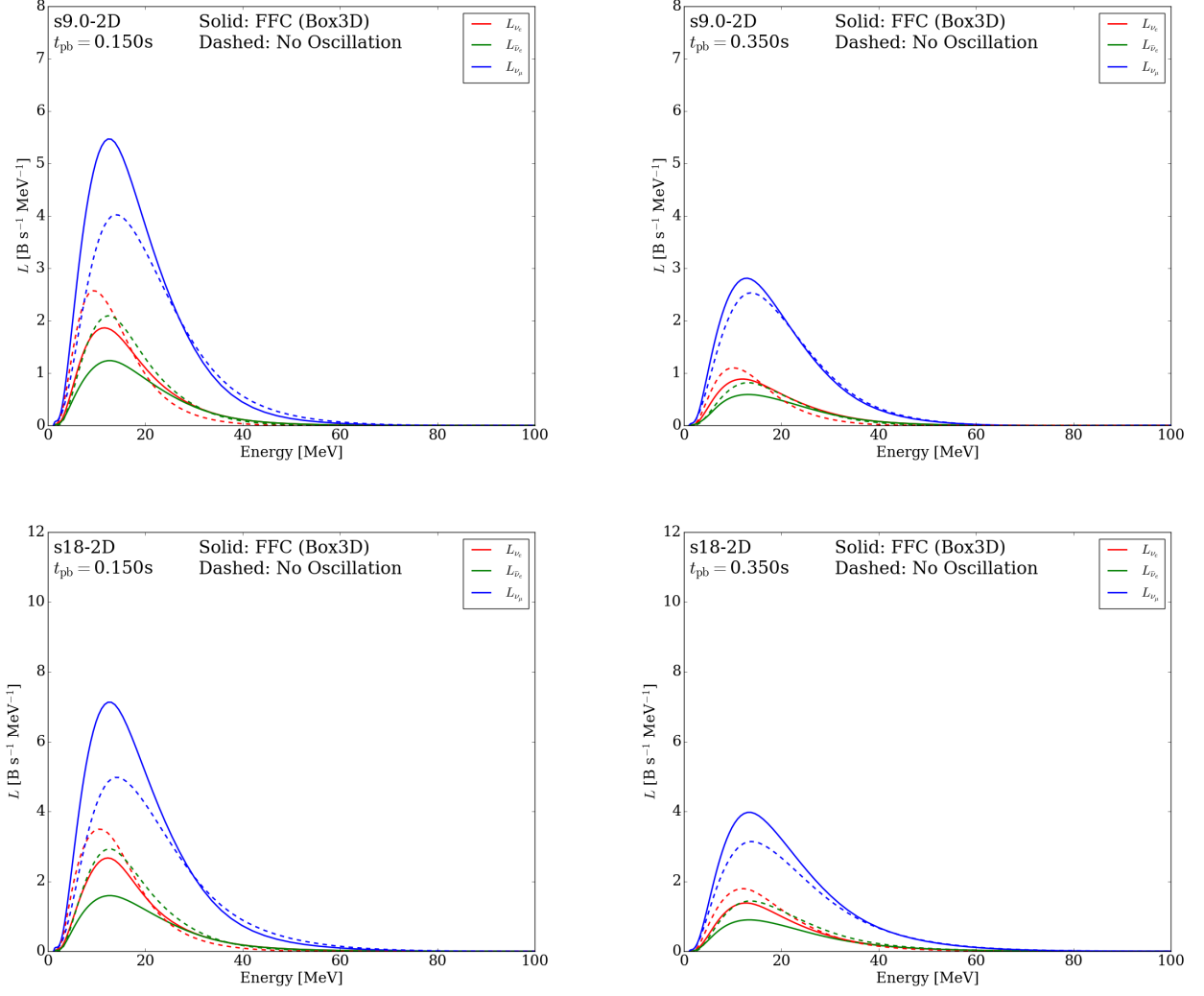


**Figure 7.** The emergent spectra (splined) of the neutrinos, with (solid) and without (dashed) the FFC, for 2D simulations of the progenitors highlighted in Figure 6 and for two times after bounce. Note that  $\nu_\mu$  is the combination of  $\nu_\mu$ ,  $\bar{\nu}_\mu$ ,  $\nu_\tau$ , and  $\bar{\nu}_\tau$ . When the FFC is operative, the  $\nu_\mu$  neutrino spectrum is softened, while both the  $\nu_e$  and  $\bar{\nu}_e$  neutrino spectra harden slightly. The net effect on the neutrino-matter heating rate is a slight enhancement (see Figures 1 and 5).

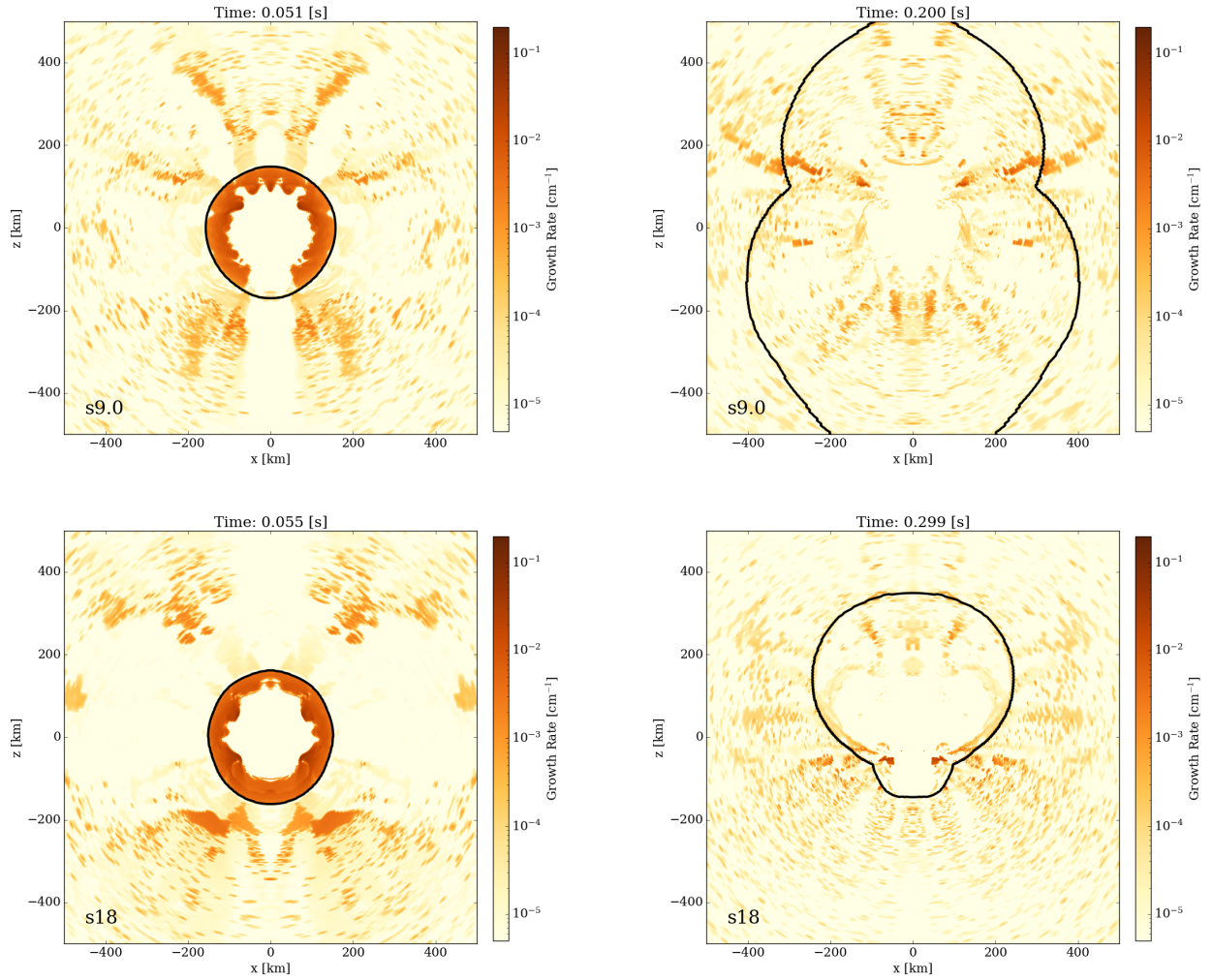


**Figure 8.** The local FFC rate (using eq. 6, in units of  $\text{cm}^{-1}$ ) for representative times after bounce for the 2D s9.0 and s18 models. The black contour shows the position of the shock. At early phases, there are FFC regions both interior and exterior to the shock, while at later phases the inner FFC region shrinks and disappears. Note the spike-like structures that are artifacts of the rings seen in 2D hydrodynamics that don't exist in 3D.

## REFERENCES

- Abbar, S., Capozzi, F., Glas, R., Janka, H. T., & Tamborra, I. 2021, *PhRvD*, 103, 063033
- Abbar, S., Duan, H., Sumiyoshi, K., Takiwaki, T., & Volpe, M. C. 2019, *PhRvD*, 100, 043004
- Arnett, D. 1967, *Canadian Journal of Physics*, 45, 1621
- Bethe, H. A., & Wilson, J. R. 1985, *ApJ*, 295, 14
- Bollig, R., Yadav, N., Kresse, D., et al. 2021, *ApJ*, 915, 28
- Bruenn, S. W., & Dineva, T. 1996, *ApJL*, 458, L71
- Burrows, A. 2013, *Reviews of Modern Physics*, 85, 245
- Burrows, A. 2018, in *Journal of Physics Conference Series*, ed. J. Dumarchez, M. Cribier, & D. Vignaud, *AstroParticle and Cosmology Laboratory (APC)*, 161–172
- Burrows, A., Hayes, J., & Fryxell, B. A. 1995a, *ApJ*, 450, 830
- . 1995b, *ApJ*, 450, 830
- Burrows, A., Radice, D., & Vartanyan, D. 2019, *MNRAS*, 485, 3153
- Burrows, A., Radice, D., Vartanyan, D., et al. 2020, *MNRAS*, 491, 2715
- Burrows, A., Reddy, S., & Thompson, T. A. 2006, *Nuclear Physics A*, 777, 356
- Burrows, A., & Vartanyan, D. 2021, *Nature*, 589, 29
- Burrows, A., Vartanyan, D., Dolence, J. C., Skinner, M. A., & Radice, D. 2018, *Space Science Reviews*, 214, 33
- Burrows, A., Vartanyan, D., & Wang, T. 2023, *ApJ*, 957, 68
- Burrows, A., Wang, T., & Vartanyan, D. 2024a, *ApJL*, 964, L16
- . 2024b, arXiv e-prints, arXiv:2412.07831
- Chakraborty, S., Hansen, R. S., Izaguirre, I., & Raffelt, G. 2016, *Journal of Cosmology and Astroparticle Physics*, 2016, 042–042.  
<http://dx.doi.org/10.1088/1475-7516/2016/03/042>
- Coleman, M. S. B., & Burrows, A. 2022, *MNRAS*, 517, 3938
- Colgate, S. A., & White, R. H. 1966, *ApJ*, 143, 626
- Ehring, J., Abbar, S., Janka, H.-T., Raffelt, G., & Tamborra, I. 2023a, *PhRvD*, 107, 103034
- . 2023b, *PhRvL*, 131, 061401
- Froustey, J., Kneller, J. P., & McLaughlin, G. C. 2024a, arXiv e-prints, arXiv:2409.05807
- Froustey, J., Richers, S., Grohs, E., et al. 2024b, *PhRvD*, 109, 043046
- George, M., Xiong, Z., Wu, M.-R., & Lin, C.-Y. 2024, *PhRvD*, 110, 123018
- Glas, R., Janka, H. T., Capozzi, F., et al. 2020, *PhRvD*, 101, 063001
- Herant, M., Benz, W., Hix, W. R., Fryer, C. L., & Colgate, S. A. 1994, *ApJ*, 435, 339
- Janka, H.-T. 2012, *Annual Review of Nuclear and Particle Science*, 62, 407
- Janka, H. T. 2025, arXiv e-prints, arXiv:2502.14836
- Janka, H. T., & Mueller, E. 1996, *A&A*, 306, 167
- Johns, L. 2023a, *PhRvL*, 130, 191001
- . 2023b, arXiv e-prints, arXiv:2306.14982
- Johns, L., & Nagakura, H. 2021, *PhRvD*, 103, 123012
- Johns, L., Nagakura, H., Fuller, G. M., & Burrows, A. 2020, *PhRvD*, 101, 043009
- Kneller, J. P., Froustey, J., Grohs, E. B., et al. 2024, arXiv e-prints, arXiv:2410.00719
- Lentz, E. J., Bruenn, S. W., Hix, W. R., et al. 2015, *ApJL*, 807, L31
- Martinez, J. G., Stovall, K., Freire, P. C. C., et al. 2015, *Astrophys. J.*, 812, 143
- Minerbo, G. N. 1978, *JQSRT*, 20, 541
- Mori, K., Takiwaki, T., Kotake, K., & Horiuchi, S. 2025, Three-dimensional core-collapse supernova models with phenomenological treatment of neutrino flavor conversions, , , arXiv:2501.15256.  
<https://arxiv.org/abs/2501.15256>
- Morinaga, T. 2022, *PhRvD*, 105, L101301
- Morinaga, T., Nagakura, H., Kato, C., & Yamada, S. 2020, *Physical Review Research*, 2, 012046
- Morozova, V., Radice, D., Burrows, A., & Vartanyan, D. 2018, *ApJ*, 861, 10
- Müller, B., Tauris, T. M., Heger, A., et al. 2019, *MNRAS*, 484, 3307
- Myers, M., Cooper, T., Warren, M., et al. 2022, *PhRvD*, 105, 123036
- Nagakura, H., Burrows, A., Johns, L., & Fuller, G. M. 2021a, *PhRvD*, 104, 083025
- Nagakura, H., Burrows, A., Radice, D., & Vartanyan, D. 2019, *MNRAS*, 490, 4622
- Nagakura, H., Burrows, A., Radice, D., & Vartanyan, D. 2020, *MNRAS*, 492, 5764
- Nagakura, H., Burrows, A., Vartanyan, D., & Radice, D. 2021b, *MNRAS*, 500, 696
- Nagakura, H., Johns, L., & Zaizen, M. 2024, *PhRvD*, 109, 083013
- Nakamura, K., Takiwaki, T., & Kotake, K. 2022, *MNRAS*, 514, 3941
- O’Connor, E., & Ott, C. D. 2011, *ApJ*, 730, 70
- Padilla-Gay, I., Tamborra, I., & Raffelt, G. G. 2022, *PhRvL*, 128, 121102
- Radice, D., Burrows, A., Vartanyan, D., Skinner, M. A., & Dolence, J. C. 2017, *ApJ*, 850, 43
- Radice, D., Morozova, V., Burrows, A., Vartanyan, D., & Nagakura, H. 2019, *ApJ*, 876, L9

- Richers, S., Duan, H., Wu, M.-R., et al. 2022, *PhRvD*, 106, 043011
- Richers, S., Froustey, J., Ghosh, S., Foucart, F., & Gomez, J. 2024, *PhRvD*, 110, 103019
- Richers, S., & Sen, M. 2022, arXiv e-prints, arXiv:2207.03561
- Richers, S., Willcox, D., & Ford, N. 2021a, *PhRvD*, 104, 103023
- Richers, S., Willcox, D. E., Ford, N. M., & Myers, A. 2021b, *PhRvD*, 103, 083013
- Richers, S. A., McLaughlin, G. C., Kneller, J. P., & Vlasenko, A. 2019, *PhRvD*, 99, 123014
- Samuel, S. 1993, *Phys. Rev. D*, 48, 1462.  
<https://link.aps.org/doi/10.1103/PhysRevD.48.1462>
- Sandoval, M. A., Hix, W. R., Messer, O. E. B., Lentz, E. J., & Harris, J. A. 2021, *ApJ*, 921, 113
- Sawyer, R. 2016, *Physical Review Letters*, 116, doi:10.1103/physrevlett.116.081101.  
<http://dx.doi.org/10.1103/PhysRevLett.116.081101>
- Sawyer, R. F. 2005, *Physical Review D*, 72, doi:10.1103/physrevd.72.045003.  
<http://dx.doi.org/10.1103/PhysRevD.72.045003>
- Skinner, M. A., Dolence, J. C., Burrows, A., Radice, D., & Vartanyan, D. 2019, *ApJS*, 241, 7
- Stanzione, D., West, J., Evans, R. T., et al. 2020, in *PEARC '20, Practice and Experience in Advanced Research Computing*, Portland, OR, 106–111
- Stapleford, C. J., Fröhlich, C., & Kneller, J. P. 2020, *PhRvD*, 102, 081301
- Steiner, A. W., Hempel, M., & Fischer, T. 2013, *ApJ*, 774, 17
- Stockinger, G., Janka, H. T., Kresse, D., et al. 2020, *MNRAS*, 496, 2039
- Strack, P., & Burrows, A. 2005, *Physical Review D*, 71, doi:10.1103/physrevd.71.093004.  
<http://dx.doi.org/10.1103/PhysRevD.71.093004>
- Sukhbold, T., Ertl, T., Woosley, S. E., Brown, J. M., & Janka, H.-T. 2016, *ApJ*, 821, 38
- Sukhbold, T., Woosley, S. E., & Heger, A. 2018, *ApJ*, 860, 93
- Vartanyan, D., & Burrows, A. 2020, *ApJ*, 901, 108
- Vartanyan, D., Burrows, A., & Radice, D. 2019a, *MNRAS*, 489, 2227
- Vartanyan, D., Burrows, A., Radice, D., Skinner, M. A., & Dolence, J. 2018, *MNRAS*, 477, 3091
- . 2019b, *MNRAS*, 482, 351
- Vartanyan, D., Burrows, A., Wang, T., Coleman, M. S. B., & White, C. J. 2023, *PhRvD*, 107, 103015
- Vartanyan, D., Coleman, M. S. B., & Burrows, A. 2022, *MNRAS*, 510, 4689
- Volpe, C. 2015, *International Journal of Modern Physics E*, 24, 1541009
- Volpe, M. C. 2024, *Reviews of Modern Physics*, 96, 025004
- Wang, T., & Burrows, A. 2020, *PhRvD*, 102, 023017
- . 2023, *ApJ*, 943, 78
- . 2024, *ApJ*, 969, 74
- Wilson, J. R. 1985, in *Numerical Astrophysics*, ed. J. M. Centrella, J. M. Leblanc, & R. L. Bowers, 422
- Xiong, Z., Wu, M.-R., Martínez-Pinedo, G., et al. 2023, *PhRvD*, 107, 083016
- Zaizen, M., Richers, S., Nagakura, H., Suzuki, H., & Kato, C. 2024, arXiv e-prints, arXiv:2407.20548
- Zhang, Y., & Burrows, A. 2013, *Physical Review D*, 88, doi:10.1103/physrevd.88.105009.  
<http://dx.doi.org/10.1103/PhysRevD.88.105009>